SHAPE DISTRIBUTION OF FRAGMENTS FROM MICROSATELLITE IMPACT TESTS

Toshiya Hanada[(1)(2)], Jer-Chyi Liou[(3)]

[(1)] Kyushu University, 744 Motooka, Nishi-ku, Fukuoka 819-0395, JAPAN, Email: toshi@aero.kyushu-u.ac.jp
[(2)] ISAS/JAXA, 3-1-1 Yoshinodai, Sagamihara, Kanagawa 229-8510, JAPAN, Email: hanada.toshiya@jaxa.jp
[(3)] NASA/JSC, Mail Code KX, 2101 NASA Parkway, Houston, TX 77058, USA, Email: jer-chyi.liou-1@nasa.gov

ABSTRACT

Fragment shape is an important factor for conducting reliable orbital debris damage assessments for critical space assets. This paper provides some information on shape distribution of fragments observed from microsatellite impact tests completed as part of an ongoing collaboration between Kyushu University and the NASA Orbital Debris Program Office. Two distinct groups can be observed in the shape distribution provided. One includes needle-like objects, while another includes plate-like objects. Therefore, this paper suggests modeling the shape distribution as two different groups, needles and plates.

1. INTRODUCTION

To date, seven microsatellite impact tests have been completed as part of an ongoing collaboration between Kyushu University and the NASA Orbital Debris Program Office (see also [1-3]). The target satellites ranged in size from 15 cm by 15 cm by 15 cm to 20 cm by 20 cm by 20 cm. Each target satellite was equipped with fully functional electronics, including circuits, battery, and transmitter. Solar panels and multi-layer insulation (MLI) were added to the target satellites of the last two tests. The impact tests were carried out with projectiles of different sizes and impact speeds.

The motivation to conduct the tests is twofold. First, as new satellite materials continue to be developed, there is a need for impact tests based on more modern materials to better characterize the outcome of future on-orbit fragmentations. Second, it is necessary to extend tests to different velocity regimes to cover potential low-velocity collisions in the geosynchronous Earth orbit region.

Fragment shape is also an important factor for conducting reliable orbital debris damage assessments for critical space assets, such as the International Space Station. All fragments down to about 2 mm in size were collected and analyzed based on their three orthogonal dimensions, x, y, and z, where x is the longest dimension, y is the longest dimension in the plane perpendicular to x, and z is the longest dimension perpendicular to both x and y. Each fragment was also photographed and classified by shape and material composition. This data set serves as the basis of our effort to develop a fragment shape distribution.

Two distinct groups can be observed in the x/y versus y/z distribution of the fragments. Objects in the first group typically have large x/y values. Many of them are needle-like objects originating from the fragmentation of carbon fiber reinforced plastic (CFRP) materials used to construct the satellites. Objects in the second group tend to have small x/y values, and many of them are box-like or plate-like objects, depending on their y/z values. Each group forms the corresponding peak in the x/y distribution. However, only one peak can be observed in the y/z distribution. These distributions and how they vary with size, material type, and impact parameters will be described in detail within the paper.

2. IMPACT EXPERIMENTS

2.1 Two-stage Light Gas Gun

All microsatellite impact tests were carried out using a two-stage light gas gun (LGG) at Kyushu Institute of Technology. The LGG is driven by gunpowder to perform an impact test. The combustion gas of the gunpowder pushes a piston to compress light gas in the first stage. Then the highly compressed light gas accelerates a projectile in the second stage right after the light gas raptures a diaphragm between the stages. The LGG has the capability to place the outcome of all microsatellite impact tests as catastrophic. The details of the LGG can be found in [4-6].

2.2 Target Microsatellites

Three different target microsatellites were prepared for the tests (see Fig. 1). The first targets were 15 cm by 15 cm by 15 cm in size and 740 grams in mass. The second and third targets were 20 cm by 20 cm by 20 cm in size, slightly larger than the first ones. As will be described later, solar panels and MLI were added to the third targets so that their mass was different; the second targets were 1300 grams in mass and the third ones were 1500 grams in mass.

As shown in Fig. 1, the main structure of each microsatellite was composed of five layers (top and bottom layers and three internal layers parallel to the top and bottom layers) and four side panels as well. They were assembled with angle bars made of an aluminum

Proc. '5th European Conference on Space Debris', Darmstadt, Germany 30 March – 2 April 2009, (ESA SP-672, July 2009)

alloy and metal spacers. The top and bottom layers and side panels were made of CFRP, while the three internal layers were made of glass fiber reinforced plastic (GFRP). The interior of each microsatellite was equipped with fully functional electronic devices, such as a wireless radio, lithium-ion batteries, and communication, electric power supply, and command and data handling circuits.

Fig. 1 also shows that the third targets had a solar panel on the top layer. The solar panel added to the third targets was an aluminum honeycomb sandwich panel with CFRP face sheets that six solar cells were mounted on. The four side panels and bottom layer were covered with a MLI. The MLI consists of six aluminum coated thermal control films and lint-free wipes slipped in between the films as spacers.

2.3 Impact Parameters

Table 1 summarizes the impact parameters of all tests. Two different size aluminum alloy solid spheres were prepared as projectiles for the first two tests (labeled HVI and LVI) in order to investigate the outcome of hypervelocity and low-velocity impacts. One projectile was 1.4 cm in diameter and 4 grams in mass to be launched at a speed of 4.44 km/s, whereas the other was 3 cm in diameter and 39 grams in mass to be launched at a speed of 1.45 km/s. For the rest, on the other hand, only the latter projectiles were prepared.

The third through fifth tests in Table 1 were carried out to investigate the effects of impact directions. Therefore, the projectile of the third and fifth tests (labeled 1 and 3, respectively) impacted perpendicular to the internal layers, whereas the projectile of the fourth tests (labeled 2) impacted parallel to the internal layers. Regarding the impact speed, the third and fourth tests (labeled 1 and 2) were the same speed (1.66 km/s), whereas the fifth test (labeled 3) was slightly faster (1.72 km/s).

The last two tests were carried out to investigate MLI and solar panel pieces. The target was oriented in such a way that the solar panel was facing to the in-coming projectile in the sixth test (labeled F). In the last test, on the other hand, the target was oriented as the solar panel was on the opposite side of the impact surface.

The ratios of impact kinetic energy to target mass for the first through sixth tests exceeded 40 J/g and the ratio for the last test was slightly below 40 J/g. NASA standard breakup model defines a collision, with a kinetic energy to target mass ratio equal to or greater than 40 J/g to be catastrophic (see [7]). Therefore, the consequences of the tests can be expected as catastrophic according to the NASA criterion.

3. DATA ANALYSIS AND DISCUSSION

3.1 Overview of Test Results

The target microsatellites were completely fragmented in all tests, consistent with the NASA prediction. Figs. 2 through 4 compare major fragments observed from each test, excluding the fifth test (labeled 3). The CFRP layer and side panel fragments are easily recognizable among the pieces. The MLI pieces are also recognizable in Fig. 4. The overall characteristics are similar, although some differences exist. As Fig. 2 shows, Shot HVI produced much more needle-like fragments, broken up from the CFRP layers and side panels, than Shot LVI did.

Fig. 3 clearly demonstrates the effects of impact directions. Even though the GFRP internal layers came out of the microsatellite, the main structure still remained in Shot 2. The projectile and fragments created had to hit the internal layers to create more and more fragments in Shot 1. On the other hand, there were no internal layers for the projectile to hit in Shot 2.

Regarding the MLI pieces, a significant difference in size and number can be observed from Fig. 4. The largest MLI piece in Shot F is similar in size to the CFRP layers or side panels, whereas larger MLI pieces were left in Shot R. The projectile hit the solar panel to create more fragments and then the created fragments expanded to damage the side panels and MLI in Shot F. On the other hand, the projectile hit the CFRP top layer to create less fragments in Shot R.

3.2. Shape Distributions

All fragments down to about 2 mm in size were collected and analyzed based on their three orthogonal dimensions, x, y, and z, where x is the longest dimension, y is the longest dimension in the plane perpendicular to x, and z is the longest dimension perpendicular to both x and y. Here we introduce the ratios x/y and y/z to discuss on fragment shape. A large x/y value represents an elongate shape, while a small value represents a planar shape. Regarding the ratio y/z, a large y/z value represents a thinner shape.

Fig. 5 indicates that there exist two distinct groups in the x/y versus y/z distributions. Objects in the first group typically have large x/y values, and many of them are needle-like. Objects in the second group tend to have small x/y values, and many of them are box-like or plate-like, depending on their y/z value.

Figs. 6 and 7 show the x/y distributions, while Figs. 8 and 9 show the y/z distributions. As shown in Figs. 6 and 7, each object group appeared in Fig. 5 forms the corresponding peaks in the x/y distribution. From Figs.

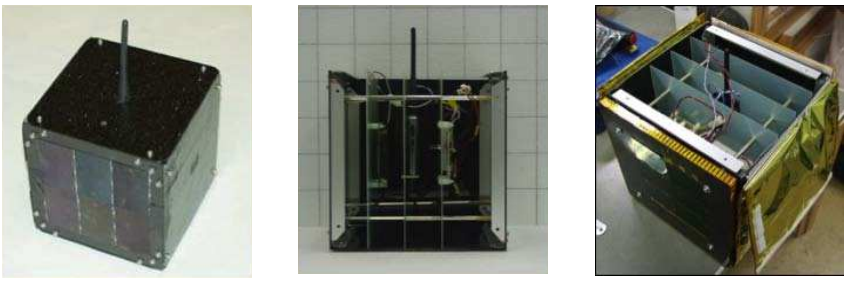

Figure 1. Target micro-satellite; (left) 15 cm by 15 cm by 15 cm in size and 740 grams in mass, (center) 20 cm by 20 cm by 20 in size and 1300 grams in mass, (right) also 20 cm by 20 cm by 20 cm but 1500 grams in mass.

Table 1. Impact parameters.

Shot	M_t [g]	M_p [g]	V_{imp} [km/s]	E_{imp} / M_t [J/g]	Impact Direction [With Respect to Layers]
HVI	740	4.03	4.44	53.7	Normal
LVI	740	39.2	1.45	55.7	Normal
1	1300	39.2	1.66	41.5	Normal
2	1283	39.2	1.66	42.0	Parallel
3	1285	39.2	1.72	45.1	Normal
F	1515	39.2	1.74	40.7	Normal
R	1525	39.3	1.78	39.3	Normal

M_t = Target Mass, M_p = Projectile Mass
V_{imp} = Impact Velocity, E_{imp} = Impact Energy (= $M_p \times V_{imp}^2 /2$)
HVI = Hypervelocity Impact, LVI = Low-velocity Impact

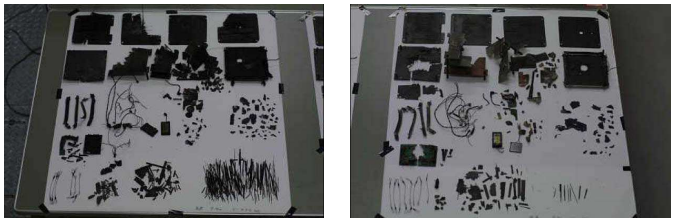

Figure 2. Fragment sets from; (left) HVI, (right) LVI.

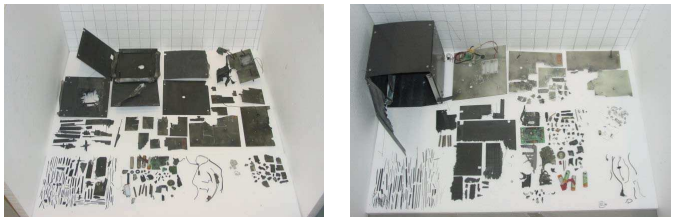

Figure 3. Fragments sets from; (left) 1, (right) 2.

Figure 4. Fragment sets from; (left) F, (right) R.

8 and 9, however, only one peak can be observed in the *y/z* distribution.

Figs. 6 and 7 show the *x/y* distributions of fragments originated from the CFRP layers and side panels as well. Figs. 6 and 7 indicates that the CFRP fragments forms the second peak from left. Again, most objects in this group (i.e. objects with larger *x/y* values) are needle-like. In addition, CFRP can be easily broken up to generate many pieces. Nowadays, CFRP is commonly adopted as satellite structures and rigid antenna reflectors. Therefore, we may expect many CFRP needles as outcome of future satellite fragmentations.

CFRP was used as the thin external layers and the side panels of the target microsatellites. Therefore, as shown in Figs. 8 and 9, CFRP fragments have relatively large *y/z* values. Figs. 8 and 9 also indicate that the CFRP fragments contribute much to form the peak in the *y/z* distribution.

Figs. 7 and 9 also show the *x/y* and *y/z* distributions of MLI pieces, respectively. Again, the MLI consists of six aluminum coated thermal control films and lint-free wipes slipped in between the films as spacers. The CFRP layers and side panels got broken up along their fiber but the MLI pieces did not. Therefore, they have relatively small *x/y* values, as shown in Fig. 7. Regarding the *y/z* distribution, on the other hand, they seem to have any *y/z* value. The films themselves are very thin so that the MLI pieces can take any shape.

4. CONCLUSIONS

This paper briefly summarized microsatellite impact tests completed as part of an ongoing collaboration between Kyushu University and the NASA Orbital Debris Program Office. All fragments down to about 2 mm in size were collected and analyzed based on their three orthogonal dimensions. Two distinct groups have been observed in the shape distribution provided. One includes needle-like objects, while another includes plate-like objects. Therefore, this paper suggests analyzing the shape distribution as two different groups, needles and plates.

ACKNOWLEDGEMENTS

The authors wish to acknowledge Professor Yasuhiro Akahoshi of Kyusyu Institute of Technology, Kitakyushu, Japan and his students for their dedicated assistance in all microsatellite impact tests.

REFERENCES

1. Hanada, T., Tsuruda, Y., Liou, J.-C. (2006). New Satellite Impact Experiments. *Orbital Debris Quarterly News* **10**(3), 4, NASA L. B. Johnson Space Center.

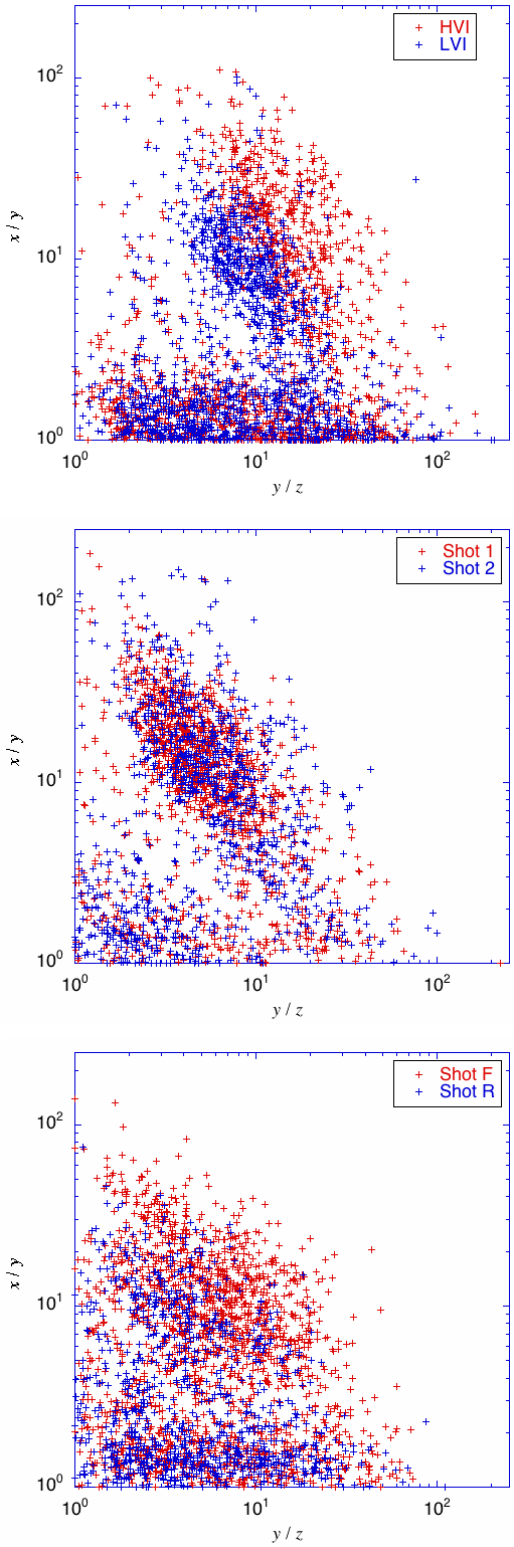

Figure 5. x/y versus y/z distributions from; (top) HVI and LVI, (middle) 1 and 2, and (bottom) F and R.

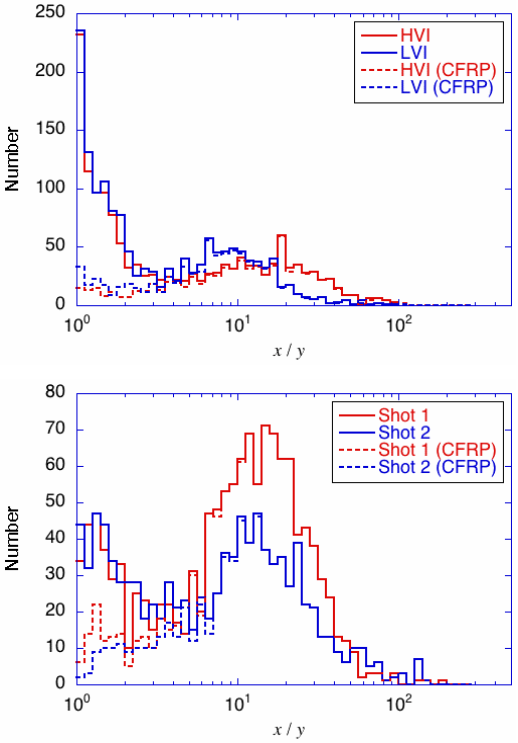

Figure 6. x/y distributions of fragments from; (top) HVI and LVI, and (bottom) 1 and 2.

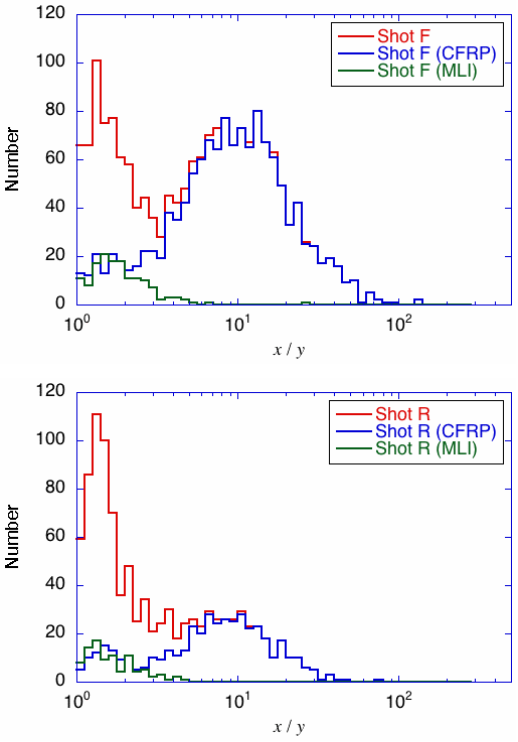

Figure 7. x/y distributions of fragments from; (top) F, and (bottom) R.

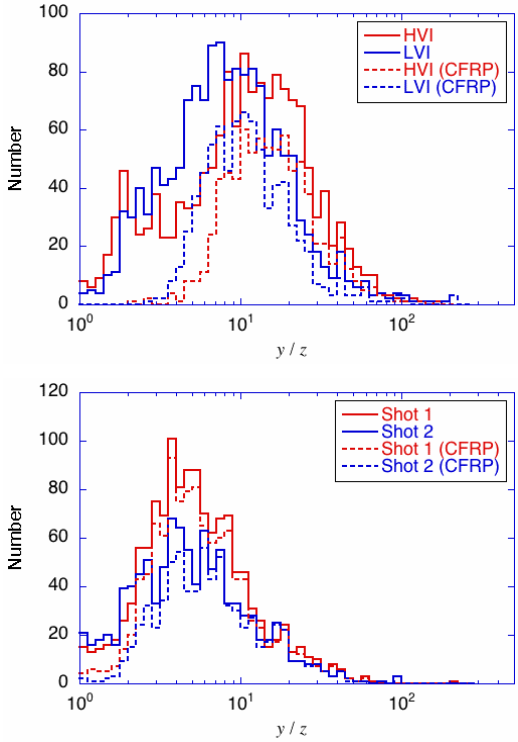

Figure 8. y/z distributions of fragments from; (top) HVI and LVI, and (bottom) 1 and 2.

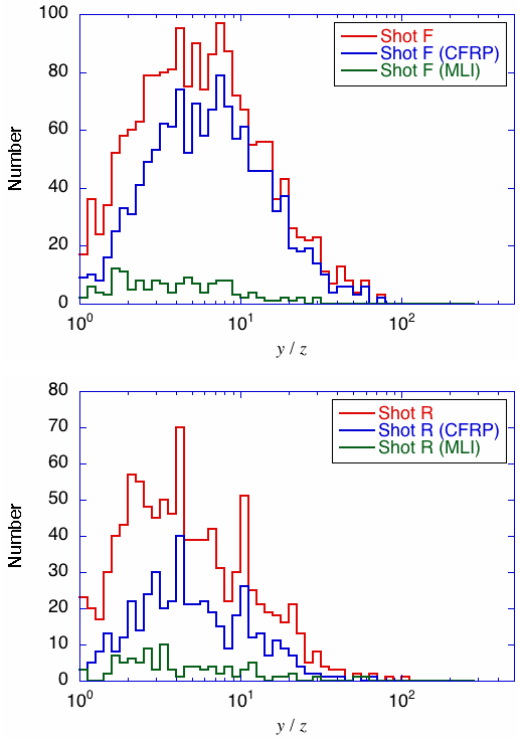

Figure 9. y/z distributions of fragments from; (top) F, and (bottom) R.

2. Hanada, T., Sakuraba, K., Liou, J.-C. (2007). Three New Satellite Impact Tests. *Orbital Debris Quarterly News* **11**(4), 4-6, NASA L. B. Johnson Space Center.

3. Murakami, J., Hanada, T., Liou, J.-C., et al. (2009). Two New Microsatellite Impact Tests in 2008. *Orbital Debris Quarterly News* **13**(1), 4-7, NASA L. B. Johnson Space Center

4. Higashide, M., Tanaka, M., Akahoshi, Y. et al. (2006). Hypervelocity Impact Tests Against Metallic Meshes. *International Journal of Impact Engineering* **33**(1-12), 335-342.

5. Kitagawa, J. (2007). Technological Development Aiming for Counter Impact by Two-stage Light Gas Gun. Master dissertation, Kyushu Institute of Technology, Kitakyushu, Japan (in Japanese).

6. Takemachi, K., Higashide, M., Akahoshi, Y. et al. (2007). Debris Cloud Distribution at Different Impact Angle. In Proc. of 2007 JSASS-KSAS Joint International Symposium on Aerospace Engineering, JSASS, Tokyo, Japan, pp.124-126.

7. Johnson, N. L., Krisko, P. H., Liou, J.-C., et al. (2001). NASA's new breakup model of EVOLVE 4.0. *Adv. Space Res.* **28**(9), 1377-1384.